

Auxiliary-field quantum Monte Carlo method with seniority-zero trial wave function

Yuichiro Yoshida,^{1,*} Luca Erhart,¹ Takuma Murokoshi,¹ Rika Nakagawa,²
Chihiro Mori,² Hanae Tagami,³ and Wataru Mizukami^{1,4,†}

¹*Center for Quantum Information and Quantum Biology, Osaka University, 1-2 Machikaneyama, Toyonaka, Osaka 560-0043, Japan*

²*Technology Strategy Center, TOPPAN Digital Inc., 1-3-3 Suido, Bunkyo-ku, Tokyo 112-8531, Japan*

³*Technical Research Institute, TOPPAN Holdings Inc., 4-2-3*

Takanodai-minami, Sugito-machi, Kita-katsushika-gun, Saitama 345-8508, Japan

⁴*Graduate School of Engineering Science, Osaka University, 1-3 Machikaneyama, Toyonaka, Osaka 560-8531, Japan*

(Dated: February 3, 2025)

We present an approach that uses the doubly occupied configuration interaction (DOCI) wave function as the trial wave functions in phaseless auxiliary-field quantum Monte Carlo (ph-AFQMC). DOCI is a seniority-zero method focused on electron pairs. Although DOCI considers much fewer electron configurations than the complete active space (CAS) configuration interaction method, it efficiently captures the static correlation, while the consequent ph-AFQMC recovers the dynamical correlation across all orbitals. We also explore an orbital-optimized version (OO-DOCI) to further improve accuracy. We test this approach on several chemical systems, including single O–H bond breaking in water and polymer additives. In these cases, OO-DOCI-AFQMC closely matches CAS-based ph-AFQMC and even outperforms coupled-cluster singles, doubles, and perturbative triples. However, for strongly correlated systems, such as the carbon dimer and multi-bond dissociation in hydrogen systems and water, the method’s accuracy drops. This suggests that seniority-zero space models may be insufficient as trial wave functions in ph-AFQMC for strongly correlated systems, suggesting the need for trial wave functions in an extended space. Despite such a limitation, our study demonstrates that DOCI- and OO-DOCI-based ph-AFQMC can reduce the steep cost of CAS approaches, offering a path to accurate multi-reference calculations for larger, more complex systems.

I. INTRODUCTION

Quantum chemical calculations have made significant advances in recent decades and have become standard practice in both computational chemistry and broader chemical research [1–5]. Single-reference (SR) methods, such as coupled-cluster singles, doubles, and perturbative triples (CCSD(T)), offer highly accurate descriptions of dynamical electron correlation for small to medium molecular systems [6, 7]. These methods are particularly effective in scenarios where the quasi-degeneracy of orbitals is not a critical factor [8]. Even for large systems, such as biomolecules, high-precision calculations are now feasible through the development of accelerated computational methods [9]. However, SR methods often fall short when dealing with systems that exhibit substantial static electron correlation, necessitating the ongoing development of multi-reference (MR) methods.

Accurate treatment of both dynamical and static electron correlation is crucial for MR systems, such as those encountered in molecular bond dissociation and transition metal complexes. Among the various approaches available, complete active space second-order perturbation theory (CASPT2) [10] is widely used to address these challenges. However, lower-order perturbation theories have limitations in capturing dynamical electron correla-

tion, highlighting the need for continued research efforts to enhance methods for accurately representing this aspect of modern quantum chemistry.

Recently, the phaseless auxiliary-field quantum Monte Carlo (ph-AFQMC) method [11] has garnered significant attention for its ability to balance high accuracy with computational efficiency [12]. This method, which operates through an imaginary-time evolution approach, has demonstrated successful applications to a wide range of systems, from molecules to solid state materials [11–15].

A notable advantage of ph-AFQMC is its reliable description of dynamical electron correlation, coupled with high parallelization efficiency. Various benchmark studies have validated its accuracy [12–17]. For example, Lee et al. showed that for datasets of SR molecular systems, ph-AFQMC is more accurate than coupled-cluster singles and doubles (CCSD) and less accurate than CCSD(T). Meanwhile, its computational cost scales from $\mathcal{O}(N^3)$ to $\mathcal{O}(N^4)$ per sample [12], where N represents the number of orbitals. This scaling offers a significant advantage over conventional approaches, where the computational costs for Møller-Plesset second-order perturbation theory (MP2), CCSD, and CCSD(T) scales as $\mathcal{O}(N^5)$, $\mathcal{O}(N^6)$, and $\mathcal{O}(N^7)$, respectively. Moreover, graphics processing unit acceleration has recently been explored for ph-AFQMC [18], further decreasing its computational time. These features highlight the promise of ph-AFQMC as a method that balances accuracy and efficiency in treating dynamical electron correlation.

Another advantage of ph-AFQMC is that it naturally

* yoshida.yuichiro.qiqb@osaka-u.ac.jp

† mizukami.wataru.qiqb@osaka-u.ac.jp

yields an MR wave function. By using an MR trial wave function, ph-AFQMC can provide a balanced treatment of systems characterized by strong electron correlation [11], making it particularly useful for problems beyond the scope of SR methods. For example, by utilizing a complete active space self-consistent field (CASSCF) trial wave function, the ph-AFQMC method has showcased precise representations of multiple bond breaking in small systems, outperforming multi-reference perturbation theories and achieving outcomes on par with multi-reference configuration interaction [12]. Challenging applications to dinuclear transition metal complexes such as $[\text{Cu}_2\text{O}_2]^{2+}$ and $[\text{Fe}_2\text{S}_2(\text{SCH}_3)]^{2-}$ have also been investigated [18, 19]. The capability of ph-AFQMC to handle both dynamical and static electron correlation renders it particularly appealing and deserving of further investigation.

However, a critical challenge arises from the exponential scaling in the preparation cost and size of the MR trial wave function in ph-AFQMC. The typical method for generating an MR wave function, such as CASSCF, incurs exponential costs owing to the combinatorial explosion required to accommodate various electronic configurations. Specifically, for a closed-shell system, the number of electronic configurations in the complete active space scales as $\binom{n}{k}^2$, where n and k represent the number of spatial orbitals and electrons per spin, respectively. This exponential growth significantly limits the feasibility of CASSCF and, by extension, the utilization of CASSCF trial wave functions within ph-AFQMC for larger systems. In fact, several studies to perform ph-AFQMC calculations using MR trial wave functions other than the complete active space (CAS) wave function have been reported in recent years [20–22], suggesting the importance of this line of research.

Doubly occupied configuration interaction (DOCI) and orbital-optimized DOCI (OO-DOCI) methods are utilized to construct MR wave functions by incorporating ground-state and pair-excited electronic configurations [23]. These so-called seniority-zero wave functions effectively capture static electron correlation [24], particularly in systems with orbital degeneracy or bond-breaking scenarios. Despite the exponential growth in preparation costs, the number of configurations is reduced to $\binom{n}{k}$ rather than $\binom{n}{k}^2$, significantly decreasing the computational prefactor and allowing for the treatment of larger active spaces.

In this study, we propose the use of DOCI and OO-DOCI wave functions as trial wave functions for ph-AFQMC to efficiently capture static electron correlation while addressing the high cost associated with MR trial wave function preparation. These methods are referred to as DOCI-AFQMC and OO-DOCI-AFQMC. Their effectiveness is demonstrated in several systems, including hydrogen systems, H_2O , and the carbon dimer. Furthermore, we showcase their applicability to industrially relevant molecular systems by investigating O–H bond dissociation in polymer additives.

The remainder of this paper is organized as follows. Sec. II provides an overview of the ph-AFQMC and DOCI methods, introducing the formalism of (OO-)DOCI-AFQMC. Section III outlines the computational procedures. Numerical results are presented in Sec. IV, with concluding remarks on the validity and limitations of the proposed methods presented in Sec. V.

II. COMPUTATIONAL METHODS

This study presents the utilization of DOCI and OO-DOCI wave functions as trial wave functions for ph-AFQMC. This section provides a brief review of both the ph-AFQMC and DOCI methods.

A. Review of ph-AFQMC

AFQMC is a method utilized to determine the electronic ground state $|\Psi_0\rangle$ of a system through imaginary-time evolution:

$$|\Psi_0\rangle = \lim_{n \rightarrow \infty} (e^{-\Delta\tau \hat{H}})^n |\Phi_0\rangle, \quad (1)$$

where $|\Phi_0\rangle$ represents an initial wave function and $\Delta\tau$ represents the imaginary time step. The operator \hat{H} denotes the fermionic Hamiltonian of the target system:

$$\hat{H} = \sum_{p,q} h_{pq} \hat{a}_p^\dagger \hat{a}_q + \frac{1}{2} \sum_{p,q,r,s} g_{psqr} \hat{a}_p^\dagger \hat{a}_q^\dagger \hat{a}_s \hat{a}_r, \quad (2)$$

where \hat{a}_p^\dagger and \hat{a}_p represent creation and annihilation operators for the p th spin-orbital, and h_{pq} and g_{psqr} denote the one- and two-electron integrals, respectively.

The two-electron integrals are factorized through Cholesky decomposition as follows:

$$g_{psqr} = \sum_l L_{ps}^l L_{qr}^l. \quad (3)$$

This method involves decomposing the two-body term in Eq. (2) into a sum of squared one-body operators. By applying a Hubbard–Stratonovich transformation, the two-body interaction is converted into a stochastic integral over auxiliary-fields, allowing the short-time propagator $e^{-\Delta\tau \hat{H}}$ to be expressed in terms of one-body operators that capture the many-body correlation effects.

In ph-AFQMC, the ground-state wave function at imaginary-time τ , $|\Psi(\tau)\rangle$, is represented as follows:

$$|\Psi(\tau)\rangle = \sum_{i=1}^{N_w} w_i \frac{|\Phi_i(\tau)\rangle}{\langle \Psi_{\text{T}} | \Phi_i(\tau) \rangle}, \quad (4)$$

where $\{|\Phi_i(\tau)\rangle\}$ represents a set of walkers, and w_i denotes the weight of i th walker, and N_w represents the total number of walkers. The state $|\Psi_{\text{T}}\rangle$ denotes the trial wave function.

A trial wave function $|\Psi_T\rangle$ is introduced to address the phase problem in the walker weights $\{w_i\}$. In brief, the weight of each walker is updated based on the overlap ratio $S_i(\tau)$:

$$w_i(\tau + \Delta\tau) \propto w_i(\tau) \cdot S_i(\tau), \quad (5)$$

where $S_i(\tau)$ is defined as follows:

$$S_i(\tau) = \frac{\langle \Psi_T | \Phi_i(\tau + \Delta\tau) \rangle}{\langle \Psi_T | \Phi_i(\tau) \rangle}. \quad (6)$$

To mitigate the phase problem, the weight is adjusted by multiplying by $\max\{0, \cos(\Delta\theta_i)\}$, where $\Delta\theta_i = \arg[S_i(\tau)]$. This adjustment effectively eliminates negative contributions that lead to numerical instabilities, as $\cos(\Delta\theta_i)$ corresponds to the real component of the overlap ratio.

By constraining the phase in this manner, ph-AFQMC prevents the uncontrolled growth of the phase problem, albeit at the cost of introducing a reliance on the trial wave function. Consequently, the accuracy of ph-AFQMC calculations is significantly influenced by the choice of $|\Psi_T\rangle$.

B. Review of DOCI

DOCI is a configuration interaction (CI) method that constructs an MR wave function using the ground-state configuration and its pair-excited configurations [23]. The DOCI wave function is expressed as follows:

$$|\Psi_{\text{DOCI}}\rangle = \sum_{i=1}^{N_{\text{DO}}} c_i \hat{s}_i | \rangle, \quad (7)$$

where $| \rangle$ denotes the vacuum state, N_{DO} represents the total number of doubly occupied (DO) electronic configurations, c_i represents the expansion coefficient of the i th DO configuration, and \hat{s}_i denotes the corresponding creation operator. Specifically,

$$\hat{s}_i = \prod_{j=1}^n \left(\hat{a}_{j\alpha}^\dagger \hat{a}_{j\beta}^\dagger \right)^{f_{ij}}, \quad (8)$$

where $\hat{a}_{j\sigma}^\dagger$ generates an electron in the j th spatial orbital with spin σ . n represents the number of spatial orbitals, and $f_{ij} \in \{0, 1\}$ indicates whether the j th orbital is doubly occupied in the i th configuration.

The total number of DO electronic configurations is expressed as:

$$N_{\text{DO}} = \binom{n}{k}, \quad (9)$$

where k represents the number of electrons of a given spin. Recall that the number of configurations in a complete active space for a closed-shell system is expressed as

$\binom{n}{k}^2$. Therefore, DOCI reduces the configuration space to the square root of that in the complete active space, allowing for the treatment of larger active spaces with fewer configurations.

A DOCI wave function is constructed from electron configurations with a seniority number $\Omega = 0$. The seniority number Ω is a measure of the number of unpaired electrons in a configuration [24]. An example of electronic configurations with different seniority numbers is shown in Figure 1. In this example, the seniority-zero

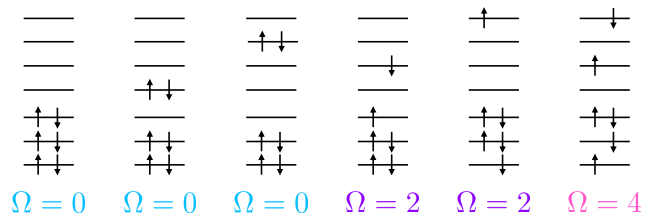


FIG. 1. Example electronic configurations and their corresponding seniority numbers.

(DOCI) wave function can encompass the three configurations on the left while excluding those on the right (which have $\Omega \neq 0$). This seniority-zero constraint effectively captures the primary electron excitations that dominate the ground-state character in many strongly correlated systems [25].

III. COMPUTATIONAL DETAILS

This section provides an overview of the computational procedures and the software utilized.

PySCF v2.2.1 [26, 27] was employed to perform self-consistent field (SCF), CCSD, CCSD(T), CASCI, and CASSCF calculations. Additionally, DOCI and OO-DOCI calculations were performed using the DOCI module for PySCF v0.1 [28]. The cc-pVDZ basis set was employed for all calculations unless otherwise specified. Density functional theory calculations were conducted using Gaussian 16 Revision C [29] for comparison.

Following the multi-configurational self-consistent field (MCSCF) calculations, ph-AFQMC calculations with the MR trial wave function were performed using ipie v0.6.2 [30].

The total imaginary-time evolution τ_{total} is defined as follows:

$$\tau_{\text{total}} = N_b \times n_s \times \Delta\tau, \quad (10)$$

where N_b and n_s represent the number of blocks and time steps, respectively. Each block serves as a unit for grouping computations to obtain energy expectation values and other observables.

Unless specified otherwise, the ph-AFQMC parameters were set as follows: time step $\Delta\tau = 0.005 E_h^{-1}$, number of steps $n_s = 50$, number of walkers $N_w = 400$, and number of blocks $N_b = 3000$.

IV. RESULTS AND DISCUSSION

A. Hydrogen chain and ring

First, we present the results for a linear H_4 chain and hexagonal H_6 ring, both of which serve as simple models of strongly correlated electron systems [31, 32].

The potential energy curve of the linear H_4 chain is shown in Figure 2. Overall, ph-AFQMC recovers the dynamical electron correlation that is absent in the bare MCSCF calculations. Particularly, OO-DOCI-AFQMC closely reproduced CASSCF-AFQMC and demonstrated good agreement with CCSD and CCSD(T).

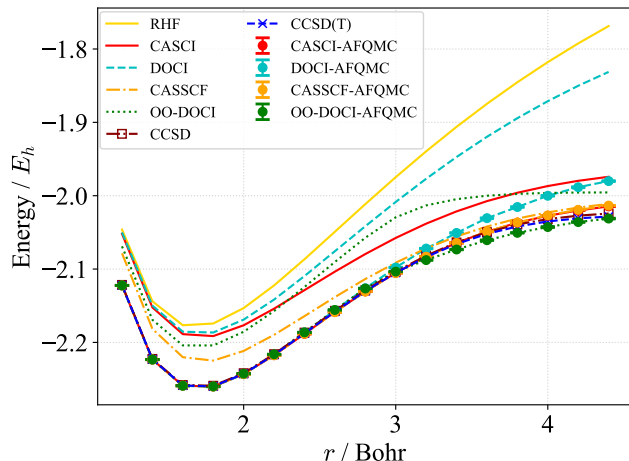


FIG. 2. Potential energy curve of the linear H_4 chain using the cc-pVDZ basis-set. The active space is (4e, 4o), with the variable r representing the distance between neighboring hydrogen atoms along the horizontal axis.

By contrast, DOCI-AFQMC overestimates the correlation energy in the dissociation region ($r > 3.0$ Bohr). This discrepancy may be attributed to the limited flexibility of the DOCI trial wave function, as the original DOCI energy curve fails to accurately capture the behavior at large bond distances.

Next, we considered the H_6 ring, with the Cartesian coordinates of the i th hydrogen atom defined as follows:

$$\mathbf{r}_i = \begin{pmatrix} x_i \\ y_i \\ z_i \end{pmatrix} = \begin{pmatrix} r \cos\left(\frac{i\pi}{3}\right) \\ r \sin\left(\frac{i\pi}{3}\right) \\ 0 \end{pmatrix}, \quad (11)$$

where $i = 0, 1, \dots, 5$. The resulting energy curves are shown in Figure 3. Similar to the H_4 case, ph-AFQMC recovers the missing dynamical electron correlation in the MCSCF calculations while capturing the strong static correlation essential for the ring dissociation. Both DOCI-AFQMC and OO-DOCI-AFQMC, utilizing MR trial wave functions, provide qualitative descriptions of dissociation and compare reasonably with CASCI-AFQMC and CASSCF-AFQMC. In contrast, the

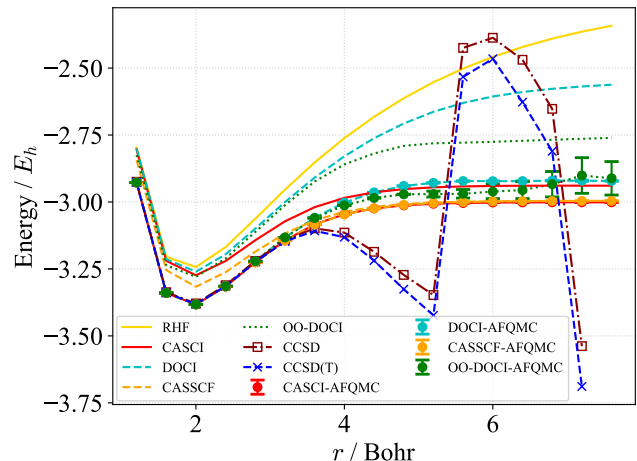


FIG. 3. Potential energy curve of the hexagonal H_6 ring using the cc-pVDZ basis-set. The active space is (6e, 6o), with the variable r representing the distance between neighboring hydrogen atoms on the horizontal axis.

single-reference CCSD and CCSD(T) break down at large r [32].

In the region, $r \geq 6$ Bohr, the standard error of OO-DOCI-AFQMC increased considerably. To investigate this phenomenon, we increased the number of walkers N_w ; the results are shown in Figure 4. We plotted graphs

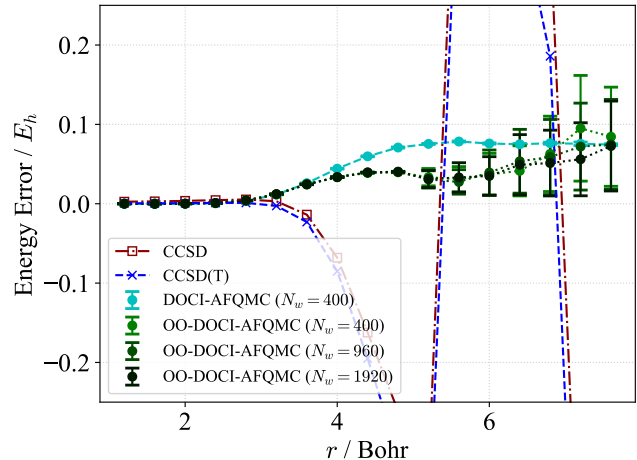


FIG. 4. Energy errors relative to CASSCF-AFQMC for the H_6 ring using the cc-pVDZ basis set. The active space is (6e, 6o), with the variable r representing the distance between neighboring hydrogen atoms along the horizontal axis.

of energy differences relative to CASSCF-AFQMC computed with $N_w = 400$. The standard error in these differences accounted for the propagated error from the reference CASSCF-AFQMC energies, which is sufficiently small (see Figure 3).

Despite increasing N_w , the standard error of OO-DOCI-AFQMC remains largely unchanged and fails to

address the issue at large values of r . Because the H_6 ring is driven by a strong static correlation, a seniority-zero wave function may not provide a fully quantitative description of the dissociation region.

B. Two O–H bond dissociation in water

Next, we examine the simultaneous stretching of the two O–H bonds in H_2O , a well-known model of double bond dissociation [33–35]. An active space of $(4e, 4o)$ was selected, comprising two a_1 and two b_2 orbitals while excluding the b_1 orbital dominated by the oxygen p -orbital perpendicular to the molecular plane. The equilibrium geometry of H_2O , utilized as the starting point for varying the two O–H bond lengths, was optimized at the MP2=FULL/cc-pVDZ level [36].

The potential energy curve for the simultaneous O–H bond dissociation is shown in Figure 5. All ph-AFQMC

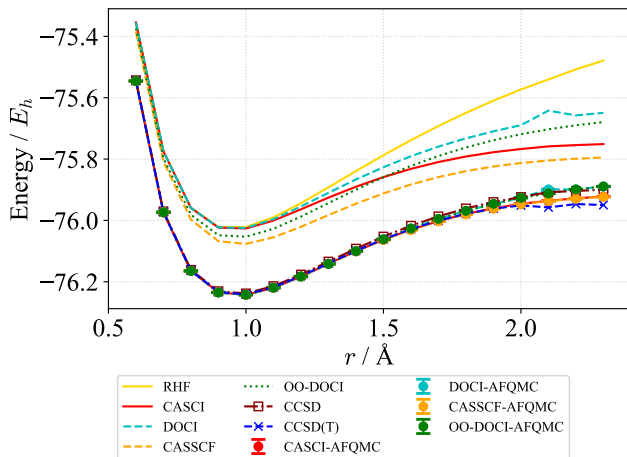


FIG. 5. Potential energy curve of the simultaneous dissociation of two O–H bonds in H_2O utilizing the cc-pVDZ basis set. The active space is $(4e, 4o)$, with the variable r representing the dissociating O–H bond length along the horizontal axis.

methods, whether utilizing CASSCF, CASCI, OO-DOCI, or DOCI trial wave functions, offer a reasonable description of the energy curve encompassing the dissociation region. Neither ph-AFQMC, CCSD, nor CCSD(T) demonstrated a significant breakdown, although minor energy variations became apparent at large r .

To highlight these differences, a graph of the deviations from CASSCF-AFQMC is shown in Figure 6. DOCI-AFQMC and OO-DOCI-AFQMC maintain chemical accuracy in structures close to the equilibrium geometry ($r \lesssim 1.5 \text{ \AA}$). However, as r surpassed 1.5 \AA , errors in both methods gradually increased, indicating that a seniority-zero trial wave function may not be adequate for a precise description of this strongly correlated regime.

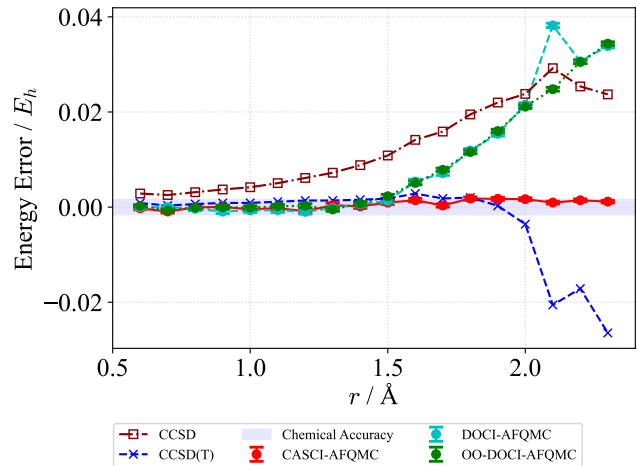


FIG. 6. Energy deviations relative to CASSCF-AFQMC for two O–H bond dissociation in H_2O using the cc-pVDZ basis set. The active space is $(4e, 4o)$, with the variable r representing the dissociating O–H bond length along the horizontal axis.

C. Carbon dimer

Subsequently, we delve into a more complex scenario: multiple bond dissociation in the carbon dimer. The potential energy curves obtained from ph-AFQMC using CASSCF($8e, 8o$), OO-DOCI($8e, 8o$), and OO-DOCI($12e, 28o$) trial wave functions are shown in Figure 7. We in-

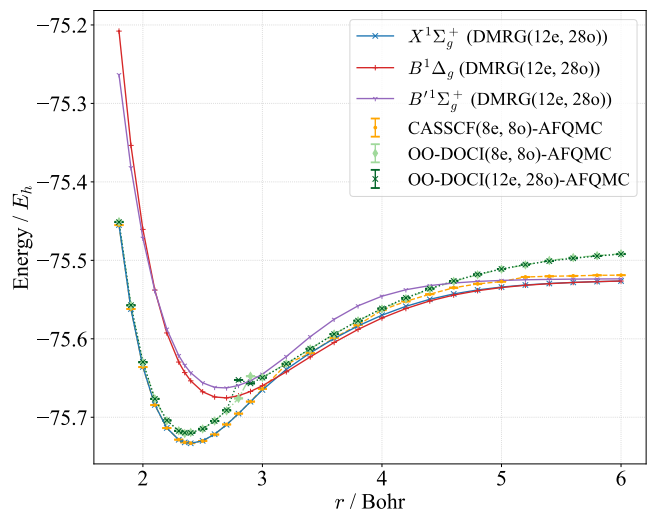


FIG. 7. Potential energy curve of the carbon dimer using the cc-pVDZ basis set. The variable r on the horizontal axis is the bond length.

corporated results from density matrix renormalization group (DMRG) calculations conducted by Wouters et al. [37] for comparison. Note that the active space $(12e, 28o)$ includes all orbitals in the cc-pVDZ basis set.

While OO-DOCI-AFQMC captured the qualitative

shape of the curve, it fell short in accuracy compared with CASSCF-AFQMC when referenced against the DMRG results. Specifically, for $r < 3.0$ Bohr, CASSCF(8e, 8o)-AFQMC closely aligned with DMRG, whereas OO-DOCI(8e, 8o)-AFQMC demonstrated significant deviations. Despite the larger active space accommodated by OO-DOCI(12e, 28o) compared with CASSCF, its energy profile closely mirrored that of OO-DOCI(8e, 8o)-AFQMC. Achieving a more precise depiction of the carbon dimer necessitates the inclusion of configurations with $\Omega > 0$ in the MR trial wave function.

The DMRG outcomes revealed a crossing point between the $X^1\Sigma_g^+$ and $B^1\Delta_g$ states around a distance of approximately $r \sim 3.1$ Bohr, whereas an avoided crossing was observed between the $X^1\Sigma_g^+$ and $B'^1\Sigma_g^+$ states. Both CASSCF-AFQMC and OO-DOCI-AFQMC demonstrated discontinuities near $r = 3.0$ Bohr, albeit at different points. This region of crossing/avoided-crossing likely triggered the observed discontinuities and has been reported in the computational investigations of frozen-pair linearized CCSD [38].

D. O–H bond dissociation in polymer additives

Finally, we examined the hydrogen dissociation from an O–H bond in three molecules: H₂O and two polymer additives (Figure 8).

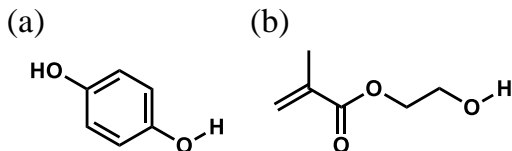


FIG. 8. Structural formulas of (a) hydroquinone (HQ) and (b) 2-hydroxyethyl methacrylate (HEMA).

The O–H dissociation energy curves for these molecules are shown in Figure 9. The relative energies were plotted, with the lowest energy point for each method serving as the reference. Standard errors for the ph-AFQMC results are shown as error bars, encompassing the propagated error from the respective reference point.

Among these three molecules examined, the bond dissociation energy ΔE followed the trend CCSD(T) < ph-AFQMC < CCSD. For HQ and HEMA, OO-DOCI-AFQMC aligned closely with CASSCF-AFQMC. For H₂O, OO-DOCI-AFQMC closely mirrored CASSCF-AFQMC and FCI results across the entire range of Figure 9 (c). Hence, OO-DOCI-AFQMC provides a highly accurate description of O–H bond dissociation.

Conversely, CCSD overestimated the bond dissociation energy, whereas CCSD(T) underestimated it. For all three molecules, the CCSD(T) energy gradually decreased in the large r region, indicating unphysical behavior. This issue with CCSD(T) will be further discussed in this study.

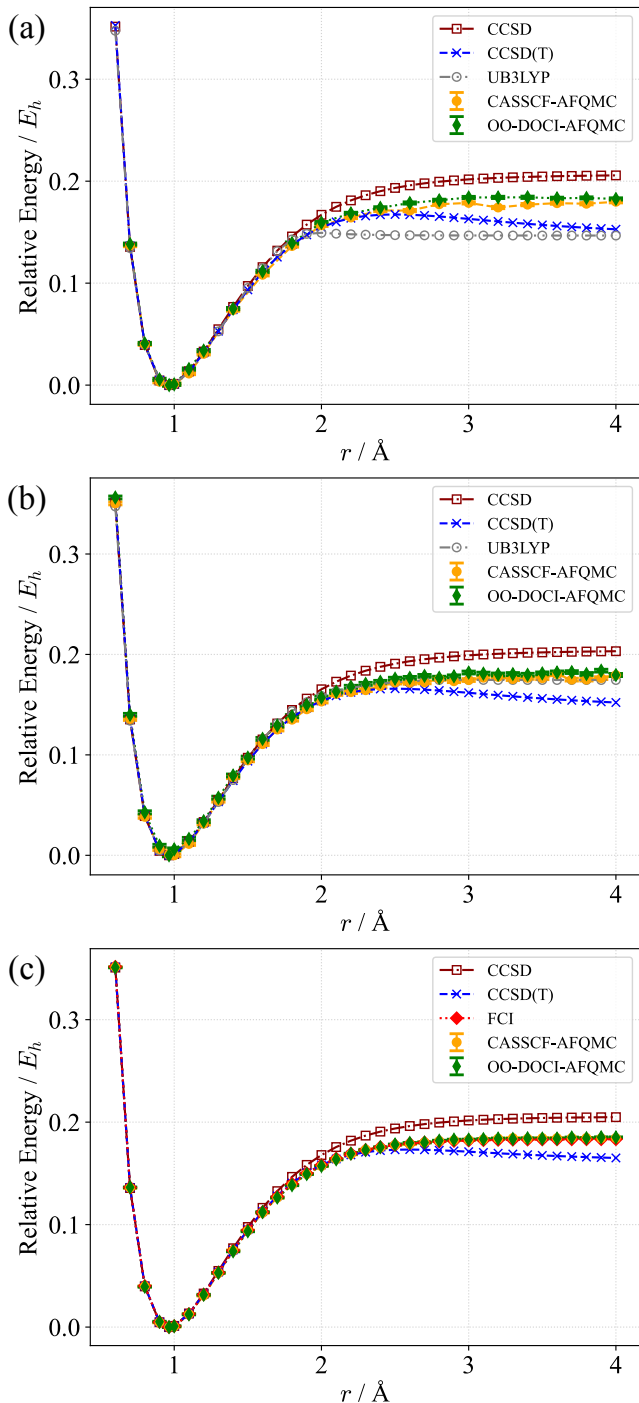


FIG. 9. Relative energy curves of (a) HQ, (b) HEMA, and (c) H₂O. The 6-31++G** basis set was used for HQ and HEMA, and the cc-pVDZ basis set for H₂O. For CASSCF and OO-DOCI, the (8e, 8o) active space was employed for HQ, whereas the (2e, 2o) for HEMA and H₂O. CCSD natural orbitals were employed for these MCSCF calculations. The variable r on the horizontal axis denotes the O–H bond distance.

Additionally, unrestricted B3LYP (UB3LYP) calculations were performed for HQ and HEMA, revealing differing trends for these two molecules. It closely aligned with ph-AFQMC for HEMA but significantly underestimated the dissociation energy for HQ.

A summary of the bond dissociation energies ΔE for each molecule is shown in Figure 10. The OO-

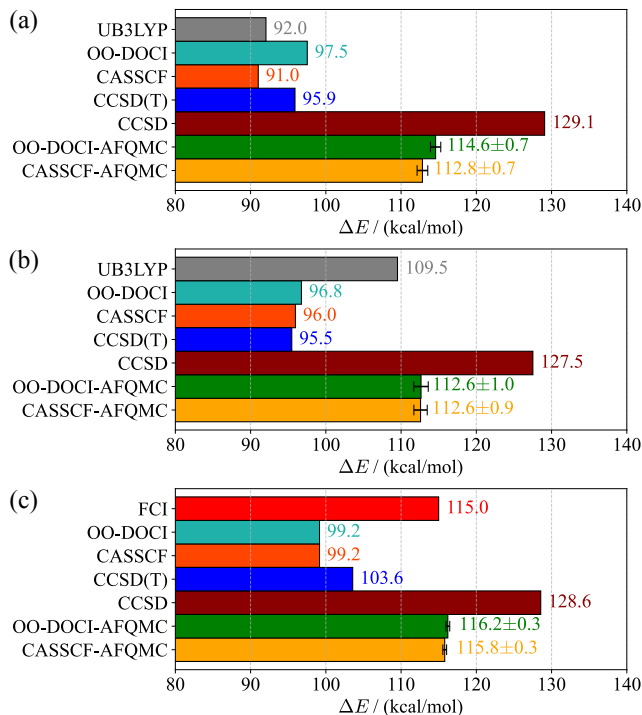


FIG. 10. O–H bond dissociation energies for (a) HQ, (b) HEMA, and (c) H_2O .

DOCI-AFQMC and CASSCF-AFQMC methods demonstrated excellent agreement and reproduced the FCI result for H_2O . These findings highlight the predictive accuracy of OO-DOCI-AFQMC in determining O–H bond dissociation energies, typically at approximately 112 kcal/mol [39].

CASSCF and OO-DOCI underestimated ΔE by more than 10 kcal/mol, underscoring the importance of recovering external electron correlation through ph-AFQMC. For HEMA and H_2O , OO-DOCI closely mirrored CASSCF due to their small (2e, 2o) active space. For HQ, however, OO-DOCI overestimated the CASSCF energy by approximately 6.5 kcal/mol due to the use of larger active space (8e, 8o), including not only the σ/σ^* orbitals of the OH bond but also the π/π^* orbitals of the nearby aromatic ring.

To gain deeper insight into the anomalous behavior of CCSD(T) in the dissociation region, we examine the T_1 diagnostic, which measures the degree of static correlation. A T_1 value exceeding 0.02 indicates that multi-reference characters can not be ignored [40].

The T_1 values for HQ and HEMA are shown in Fig-

ure 11. In both molecules, T_1 increased with the bond

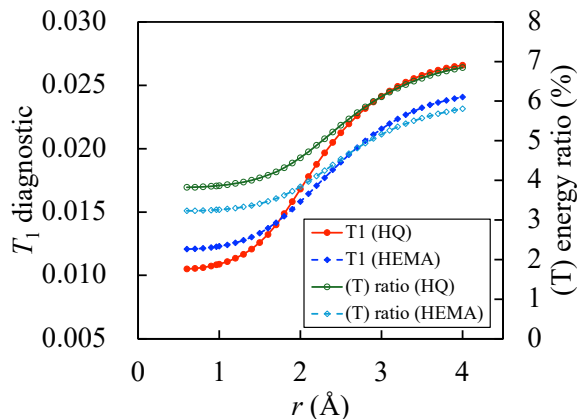


FIG. 11. T_1 diagnostic and (T) correlation energy ratios for HQ and HEMA.

length r and eventually surpassed 0.02. Similar trends are observed with the 6-311++G** basis set, although the results are omitted.

The (T) term is a perturbative correction that accounts for triple excitation contributions. As shown in Figure 11, the fraction of the total correlation energy stemming from (T) also increased with r , reflecting the growing reliance on this perturbative correction. Combined with the increasing T_1 , these observations underline the limitations of an SR approach in CCSD(T) for describing bond dissociation, thus highlighting the need for MR methods.

Finally, while the unrestricted approach in UB3LYP can qualitatively treat single-bond dissociation by allowing spin symmetry breaking, the resulting wave function is not necessarily an eigenfunction of the spin-squared operator S^2 . Figure 12 plots $\langle S^2 \rangle$ for UB3LYP wave functions of HQ and HEMA, revealing the spin contamination at large r .

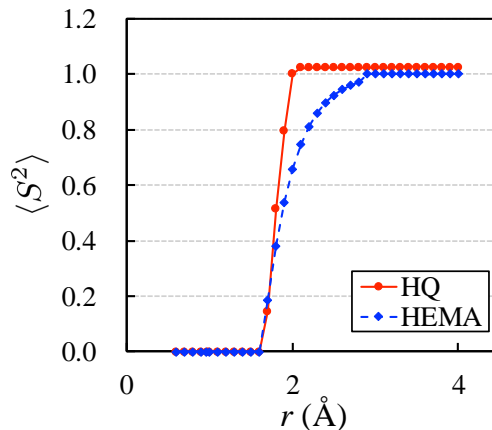


FIG. 12. Spin contamination in UB3LYP for HQ and HEMA, measured by $\langle S^2 \rangle$.

In summary, although UB3LYP can handle single-bond dissociation to a certain extent, it is plagued by spin contamination issues. Conversely, our MR methods provide a more reliable description of O–H bond dissociation.

V. CONCLUSIONS

This study proposed DOCI-/OO-DOCI-AFQMC methods that utilized DOCI-/OO-DOCI wave functions as trial wave functions for ph-AFQMC. These seniority-zero wave functions efficiently captured static electron correlation using only the ground-state and the pair-excited configurations, thereby requiring significantly fewer electronic configurations than CAS-based methods.

This approach allowed ph-AFQMC to use MR trial wave functions beyond the typical limit of about 16 electrons in 16 orbitals by reducing the exponential overhead associated with CAS methods. A key objective was to investigate the extent to which ph-AFQMC can recover the missing correlation when the trial wave function is restricted to the seniority-zero space.

Numerical results demonstrated that OO-DOCI-AFQMC closely aligned with CASSCF-AFQMC for single O–H bond dissociation and showed good agreement with FCI for the H₂O scenario, suggesting reliability for other single-bond dissociation processes.

For multiple bond dissociations, DOCI-/OO-DOCI-AFQMC successfully reproduced CASCI-/CASSCF-AFQMC near equilibrium and at intermediate bond

lengths, except for the carbon dimer case. However, ph-AFQMC calculations using seniority-zero trial wave functions may lack quantitative accuracy in the fully dissociated regime, highlighting limitations for strongly correlated systems.

Therefore, expanding the seniority space is crucial for enhancing the accuracy of MR wave function-based ph-AFQMC in multiple-bond dissociation. As a similar approach to our study, other seniority-zero methods, such as the pair coupled-cluster method [25, 41, 42], are also worth trying. Furthermore, applying this approach to other MR systems requiring larger active spaces, such as polynuclear transition metal complexes, holds promise for future research.

ACKNOWLEDGEMENTS

We thank Nobuki Inoue for fruitful discussion. We also thank Shigeki Furukawa for providing experimental data on polymer additives. This project was supported by funding from the MEXT Quantum Leap Flagship Program (MEXTQLEAP) through Grant No. JPMXS0120319794, and the JST COI-NEXT Program through Grant No. JPMJPF2014. The completion of this research was partially facilitated by the JSPS Grants-in-Aid for Scientific Research (KAKENHI), specifically Grant Nos. JP23H03819. Some of the results were obtained using the computational resources of the AI Bridging Cloud Infrastructure (ABCI) provided by National Institute of Advanced Industrial Science and Technology (AIST).

-
- [1] K. Burke, Perspective on density functional theory, *J. Chem. Phys.* **136**, 150901 (2012).
- [2] R. O. Jones, Density functional theory: Its origins, rise to prominence, and future, *Rev. Mod. Phys.* **87**, 897 (2015).
- [3] L. Chanussot, A. Das, S. Goyal, T. Lavril, M. Shuaibi, M. Riviere, K. Tran, J. Heras-Domingo, C. Ho, W. Hu, A. Palizhati, A. Sriram, B. Wood, J. Yoon, D. Parikh, C. L. Zitnick, and Z. Ulissi, Open catalyst 2020 (oc20) dataset and community challenges, *ACS Catal.* **11**, 6059 (2021).
- [4] L. Barroso-Luque, M. Shuaibi, X. Fu, B. M. Wood, M. Dzamba, M. Gao, A. Rizvi, C. L. Zitnick, and Z. W. Ulissi, Open materials 2024 (omat24) inorganic materials dataset and models (2024), arXiv:2410.12771 [cond-mat.mtrl-sci].
- [5] A. Merchant, S. Batzner, S. S. Schoenholz, M. Aykol, G. Cheon, and E. D. Cubuk, Scaling deep learning for materials discovery, *Nature* **624**, 80 (2023).
- [6] J. S. Smith, B. T. Nebgen, R. Zubatyuk, N. Lubbers, C. Devereux, K. Barros, S. Tretiak, O. Isayev, and A. E. Roitberg, Approaching coupled cluster accuracy with a general-purpose neural network potential through transfer learning, *Nat. Commun.* **10**, 2903 (2019).
- [7] D. M. Wilkins, A. Grisafi, Y. Yang, K. U. Lao, R. A. DiStasio, and M. Ceriotti, Accurate molecular polarizabilities with coupled cluster theory and machine learning, *Proceedings of the National Academy of Sciences* **116**, 3401 (2019).
- [8] D. I. Lyakh, M. Musiał, V. F. Lotrich, and R. J. Bartlett, Multireference nature of chemistry: The coupled-cluster view, *Chem. Rev.* **112**, 182 (2012).
- [9] C. Riplinger, B. Sandhoefer, A. Hansen, and F. Neese, Natural triple excitations in local coupled cluster calculations with pair natural orbitals, *J. Chem. Phys.* **139**, 134101 (2013).
- [10] K. Andersson, P. Malmqvist, and B. O. Roos, Second-order perturbation theory with a complete active space self-consistent field reference function, *J. Chem. Phys.* **96**, 1218 (1992).
- [11] S. Zhang and H. Krakauer, Quantum Monte Carlo Method using Phase-Free Random Walks with Slater Determinants, *Phys. Rev. Lett.* **90**, 136401 (2003).
- [12] J. Lee, H. Q. Pham, and D. R. Reichman, Twenty years of auxiliary-field quantum monte carlo in quantum chemistry: An overview and assessment on main group chemistry and bond-breaking, *J. Chem. Theory Comput.* **18**, 7024 (2022).

- [13] A. Taheridehkordi, M. Schlipf, Z. Sukurma, M. Humer, A. Grüneis, and G. Kresse, Phaseless auxiliary field quantum Monte Carlo with projector-augmented wave method for solids, *J. Chem. Phys.* **159**, 044109 (2023).
- [14] J. Lee, F. D. Malone, and M. A. Morales, An auxiliary-field quantum Monte Carlo perspective on the ground state of the dense uniform electron gas: An investigation with Hartree-Fock trial wavefunctions, *J. Chem. Phys.* **151**, 064122 (2019).
- [15] H. Neugebauer, H. T. Vuong, J. L. Weber, R. A. Friesner, J. Shee, and A. Hansen, Toward Benchmark-Quality Ab Initio Predictions for 3d Transition Metal Electrocatalysts: A Comparison of CCSD(T) and ph-AFQMC, *J. Chem. Theory Comput.* **19**, 6208 (2023).
- [16] Z. Sukurma, M. Schlipf, M. Humer, A. Taheridehkordi, and G. Kresse, Benchmark Phaseless Auxiliary-Field Quantum Monte Carlo Method for Small Molecules, *J. Chem. Theory Comput.* **19**, 4921 (2023).
- [17] Y. Wei, S. Debnath, J. L. Weber, A. Mahajan, D. R. Reichman, and R. A. Friesner, Scalable Ab Initio Electronic Structure Methods with Near Chemical Accuracy for Main Group Chemistry, *J. Phys. Chem. A* **128**, 5796 (2024).
- [18] Y. Huang, Z. Guo, H. Q. Pham, and D. Lv, GPU-accelerated Auxiliary-field quantum Monte Carlo with multi-Slater determinant trial states, arXiv e-prints 10.48550/arXiv.2406.08314 (2024), arXiv:2406.08314 [physics.chem-ph].
- [19] A. Mahajan and S. Sharma, Taming the sign problem in auxiliary-field quantum monte carlo using accurate wave functions, *J. Chem. Theory Comput.* **17**, 4786 (2021).
- [20] A. Mahajan, J. Lee, and S. Sharma, Selected configuration interaction wave functions in phaseless auxiliary field quantum Monte Carlo, *J. Chem. Phys.* **156**, 174111 (2022).
- [21] A. Mahajan, J. H. Thorpe, J. S. Kurian, D. R. Reichman, D. A. Matthews, and S. Sharma, Beyond CCSD(T) accuracy at lower scaling with auxiliary field quantum Monte Carlo, arXiv e-prints , arXiv:2410.02885 (2024), arXiv:2410.02885 [physics.chem-ph].
- [22] T. Jiang, B. O’Gorman, A. Mahajan, and J. Lee, Unbiasing fermionic auxiliary-field quantum Monte Carlo with matrix product state trial wavefunctions, *Phys. Rev. Res.* **7**, 013038 (2025).
- [23] F. Weinhold and J. Wilson, E. Bright, Reduced Density Matrices of Atoms and Molecules. I. The 2 Matrix of Double-Occupancy, Configuration-Interaction Wavefunctions for Singlet States, *J. Chem. Phys.* **46**, 2752 (1967).
- [24] L. Bytautas, T. M. Henderson, C. A. Jiménez-Hoyos, J. K. Ellis, and G. E. Scuseria, Seniority and orbital symmetry as tools for establishing a full configuration interaction hierarchy, *J. Chem. Phys.* **135**, 044119 (2011).
- [25] T. Stein, T. M. Henderson, and G. E. Scuseria, Seniority zero pair coupled cluster doubles theory, *J. Chem. Phys.* **140**, 214113 (2014).
- [26] Q. Sun, X. Zhang, S. Banerjee, P. Bao, M. Barbry, N. S. Blunt, N. A. Bogdanov, G. H. Booth, J. Chen, Z.-H. Cui, J. J. Eriksen, Y. Gao, S. Guo, J. Hermann, M. R. Hermes, K. Koh, P. Koval, S. Lehtola, Z. Li, J. Liu, N. Mardirossian, J. D. McClain, M. Motta, B. Mussard, H. Q. Pham, A. Pulkin, W. Purwanto, P. J. Robinson, E. Ronca, E. R. Sayfutyarova, M. Scheurer, H. F. Schurkus, J. E. T. Smith, C. Sun, S.-N. Sun, S. Upadhyay, L. K. Wagner, X. Wang, A. White, J. D. Whitfield, M. J. Williamson, S. Wouters, J. Yang, J. M. Yu, T. Zhu, T. C. Berkelbach, S. Sharma, A. Y. Sokolov, and G. K.-L. Chan, Recent developments in the PySCF program package, *J. Chem. Phys.* **153**, 024109 (2020).
- [27] Q. Sun, T. C. Berkelbach, N. S. Blunt, G. H. Booth, S. Guo, Z. Li, J. Liu, J. D. McClain, E. R. Sayfutyarova, S. Sharma, S. Wouters, and G. K.-L. Chan, Pyscf: the python-based simulations of chemistry framework, *WIREs Comput. Mol. Sci.* **8**, e1340 (2018).
- [28] Q. Sun, DOCI module for PySCF (2021).
- [29] M. J. Frisch, G. W. Trucks, H. B. Schlegel, G. E. Scuseria, M. A. Robb, J. R. Cheeseman, G. Scalmani, V. Barone, G. A. Petersson, H. Nakatsuji, X. Li, M. Caricato, A. V. Marenich, J. Bloino, B. G. Janesko, R. Gomperts, B. Mennucci, H. P. Hratchian, J. V. Ortiz, A. F. Izmaylov, J. L. Sonnenberg, D. Williams-Yong, F. Ding, F. Lipparini, F. Egidi, J. Goings, B. Peng, A. Petrone, T. Henderson, D. Ranasinghe, V. G. Zakrzewski, J. Gao, N. Rega, G. Zheng, W. Liang, M. Hada, M. Ehara, K. Toyota, R. Fukuda, J. Hasegawa, M. Ishida, T. Nakajima, Y. Honda, O. Kitao, H. Nakai, T. Vreven, K. Throssell, J. A. Montgomery, Jr., J. E. Peralta, F. Ogliaro, M. J. Bearpark, J. J. Heyd, E. N. Brothers, K. N. Kudin, V. N. Staroverov, T. A. Keith, R. Kobayashi, J. Normand, K. Raghavachari, A. P. Rendell, J. C. Burant, S. S. Iyengar, J. Tomasi, M. Cossi, J. M. Millam, M. Klene, C. Adamo, R. Cammi, J. W. Ochterski, R. L. Martin, K. Morokuma, O. Farkas, J. B. Foresman, and D. J. Fox, Gaussian 16 Revision C.02 (2016), Gaussian Inc. Wallingford CT.
- [30] F. D. Malone, A. Mahajan, J. S. Spencer, and J. Lee, ipie: A Python-Based Auxiliary-Field Quantum Monte Carlo Program with Flexibility and Efficiency on CPUs and GPUs, *J. Chem. Theory Comput.* **19**, 109 (2023).
- [31] A. V. Sinitskiy, L. Greenman, and D. A. Mazziotti, Strong correlation in hydrogen chains and lattices using the variational two-electron reduced density matrix method, *J. Chem. Phys.* **133**, 014104 (2010).
- [32] D. Kats and F. R. Manby, Communication: The distinguishable cluster approximation, *J. Chem. Phys.* **139**, 021102 (2013).
- [33] T. M. Henderson, I. W. Bulik, T. Stein, and G. E. Scuseria, Seniority-based coupled cluster theory, *J. Chem. Phys.* **141**, 244104 (2014).
- [34] T. Kinoshita, O. Hino, and R. J. Bartlett, Coupled-cluster method tailored by configuration interaction, *J. Chem. Phys.* **123**, 074106 (2005).
- [35] L. Erhart, Y. Yoshida, V. Khinevich, and W. Mizukami, Coupled cluster method tailored with quantum computing, *Phys. Rev. Res.* **6**, 023230 (2024).
- [36] R. D. J. III, Nist computational chemistry comparison and benchmark database, <http://cccbdb.nist.gov/> (2022), nIST Standard Reference Database Number 101, Release 22, May 2022.
- [37] S. Wouters, W. Poelmans, P. W. Ayers, and D. Van Neck, CheMPS2: A free open-source spin-adapted implementation of the density matrix renormalization group for ab initio quantum chemistry, *Comput. Phys. Commun.* **185**, 1501 (2014).
- [38] A. Leszczyk, M. Máté, Ö. Legeza, and K. Boguslawski, Assessing the accuracy of tailored coupled cluster methods corrected by electronic wave functions of polynomial cost, *J. Chem. Theory Comput.* **18**, 96 (2022).

- [39] Bond Energies (2023), [Online; accessed 2024-11-03].
- [40] T. J. Lee and P. R. Taylor, A diagnostic for determining the quality of single-reference electron correlation methods, *Int. J. Quantum Chem.* **36**, 199 (1989).
- [41] P. A. Limacher, P. W. Ayers, P. A. Johnson, S. De Baerdemacker, D. Van Neck, and P. Bultinck, A New Mean-Field Method Suitable for Strongly Correlated Electrons: Computationally Facile Antisymmetric Products of Nonorthogonal Geminals, *J. Chem. Theory Comput.* **9**, 1394 (2013).
- [42] K. Boguslawski, P. Tecmer, P. W. Ayers, P. Bultinck, S. De Baerdemacker, and D. Van Neck, Efficient description of strongly correlated electrons with mean-field cost, *Phys. Rev. B* **89**, 201106 (2014).